RSC Advances

Chemical Looping Beyond Combustion: Production of Synthesis Gas via Chemical Looping Partial Oxidation of Methane

Journal:	*RSC Advances*
Manuscript ID:	RA-ART-06-2014-006437.R1
Article Type:	Paper
Date Submitted by the Author:	16-Sep-2014
Complete List of Authors:	Bhavsar, Saurabh; University of Pittsburgh, Chemical Engineering Department; U.S. Department of Energy – National Energy Technology Laboratory, Veser, Götz; University of Pittsburgh, Chemical Engineering Department; U.S. Department of Energy – National Energy Technology Laboratory,

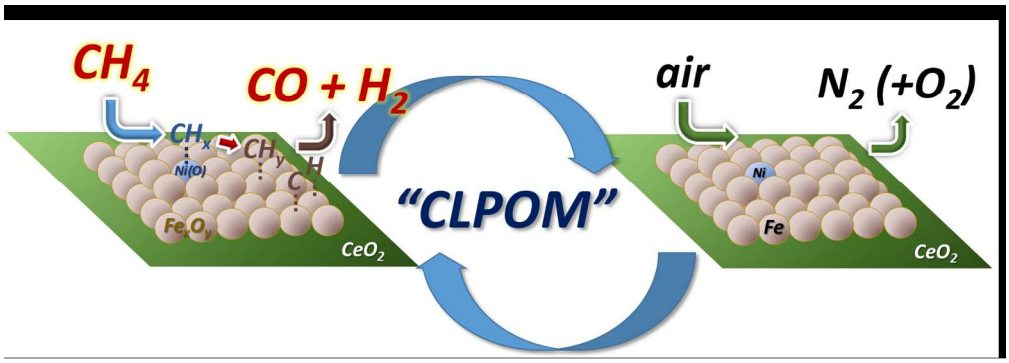

Systematic development of Fe-Ni bimetallic carrier results in efficient and safe chemical looping process for methane partial oxidation to syngas.

Chemical Looping Beyond Combustion: Production of Synthesis Gas via Chemical Looping Partial Oxidation of Methane

Saurabh Bhavsar[1,2] and Götz Veser[1,2,*]

[1] *Chemical Engineering Department, Swanson School of Engineering, University of Pittsburgh, Pittsburgh, PA 15261*

[2] *U.S. Department of Energy – National Energy Technology Laboratory, Pittsburgh, PA*

Abstract:

The recent surge in natural gas reserves has revived interest in the development of novel processes to convert natural gas into valuable chemical feedstocks. In the present work, we are applying "chemical looping", a technology that has found much attention as a clean combustion technology, towards selective partial oxidation of methane (CLPOM) to produce synthesis gas. By tailoring the composition of Ni_xFe_{1-x}-CeO_2 oxygen carriers and carefully controlling the supply of oxygen, i.e., the extent of the carrier reduction and oxidation in redox cycles, the reactivity and selectivity of these carriers for partial oxidation was optimized. Addition of a small amount of Ni to iron oxides allowed to combine the high reactivity of Ni for methane activation with the good syngas selectivity of iron oxides. An optimized carrier with the composition of $Ni_{0.12}Fe_{0.88}$-CeO_2 demonstrated excellent stability in multi-cycle CLPOM operation and high syngas yields with a H_2:CO ratio of ~2 and minimal carbon formation. Finally, a simplified fixed-bed reactor model was used to assess the thermal aspects of operating the process in a periodically operated fixed-bed reactor. We found that the process is highly sensitive to the degree of carrier utilization, but that maximum temperatures can be easily

* Corresponding Author: Prof. Götz Veser (gveser@pitt.edu)

controlled in CLPOM via control of the active metal content and oxygen utilization in the carriers. Overall, chemical looping partial oxidation of methane emerges as an attractive alternative to conventional catalytic partial oxidation, enabling the use of low-cost transition metal oxides and air as oxidant, and resulting in inherently safe reactor operation by avoiding mixed methane/air streams.

Keywords:

Chemical looping, partial oxidation, synthesis gas, iron, nickel, mixed oxides, ceria.

1. Introduction:

Sustainable production of chemicals and supply of clean energy is of paramount importance to reduce our environmental foot-print and mitigate escalating anthropogenic CO_2 emissions, the majority of which result from energy production via combustion of carbon-based fossil fuels[1]. While a transition to renewable resources hence needs to be our long-term goal, the development of bridging technologies which can provide rapidly deployable solutions is necessary to efficiently address these concerns in the immediate future. The vast natural gas resources which have become economically accessible due to advances in drilling technology have made natural gas one of the most promising bridge fuels and, as a consequence, domestic natural gas reserves are expected to almost double the in near future[2].

In parallel, over the last two decades, chemical looping combustion (CLC), an elegant technology that can be retrofitted to the current power producing infrastructure, has emerged as one of the most promising solutions for energy production from fossil (or renewable) fuels with inherent CO_2 capture[3-5]. In CLC, combustion of a fuel is broken down into two spatially separated steps: An oxygen carrier (typically a metal oxide) is contacted with fuel in a first reactor (fuel reactor), undergoing reduction while providing the oxygen necessary for fuel combustion. After combustion, the reduced metal is transferred to a second reactor (air reactor) where it is re-oxidized in contact with air. The (re-)oxidized metal is then circulated back into the fuel reactor, completing the materials 'loop'. In the fuel reactor, combustion, i.e. total oxidation of methane is targeted to yield a pure stream of CO_2 and H_2O as reactor effluent from which high-concentration, sequestration ready CO_2 can be readily obtained via condensation of steam. In this way CLC enables an efficient route for clean, flameless and NO_x-lean combustion with

minimal efficiency penalty for CO_2 capture, making it rather unique among current emerging technologies[6-9].

Beyond using the abundant supply of locally available natural gas for combustion, interest in using this resource for the production of chemicals and liquid fuels is rapidly increasing. However, direct conversion of methane to chemicals remains elusive to-date, and any industrial scale conversion of methane to chemicals presently proceeds via synthesis gas (or "syngas", a mixture of CO and H_2) as an intermediate. Industrial production of synthesis gas from methane is a mature technology, currently almost exclusively based on steam reforming of methane (SRM) ($CH_4 + H_2O = CO + 3\ H_2$; $\Delta H_R = +206$ kJ/mol). However, SRM is an energy intensive process due to the endothermic nature of the reaction as well as the necessary down-stream processing required to achieve a H_2:CO ratio of 2 (desired for most major downstream processes). In recent decades, catalytic partial oxidation of methane (CPOM) has therefore received much attention as a promising alternative[10-12]. In CPOM, methane is converted directly with oxygen to syngas over a noble metal catalyst in a simple, one step reaction: $CH_4 + ½\ O_2 = CO + 2\ H_2$ ($\Delta H_R = -37$ kJ/mol)[13]. The system is characterized by a high autothermal temperature exceeding 1000°C, which results in high reaction rates and hence extremely short contact times[10]. Overall, CPOM offers several advantages over SRM, including the exothermicity of the reaction which allows for autothermal operation (rendering external heat supply unnecessary), thus also lowering the carbon footprint of syngas production, and the very high reaction rates which allow for compact reactors with very high space-time yields. However, while CPOM is fundamentally an attractive alternative to SRM, several issues have so far significantly hampered its industrial implementation. These include safety concerns due to contacting fuel with oxygen at high

temperatures close to their upper flammability limit; the need for an air separation unit to produce undiluted streams of syngas; and the use of expensive noble metal catalysts.

The "chemical looping" principle offers an opportunity to directly address several of these issues: The spatial separation of the fuel conversion into two separate half-steps completely avoids any direct contact between the fuel and the oxidizing gas and hence alleviates safety concerns. At the same time, the air separation that is intrinsic to looping processes allows utilization of air without the use of an external air separation unit and without resulting in N_2 dilution of the produced syngas.

Chemical looping thus enables a novel process configuration for syngas production which can be realized in at least two different ways: In one configuration, which constitutes only a minor modification from chemical looping combustion, steam is co-fed with methane in the fuel reactor, resulting in methane reforming with the difference that the reaction heat is coupled directly into the reactor volume via the (hot) oxygen carriers, avoiding the inefficiencies of external firing large-scale reactors. The resulting net process yields the looping equivalent of autothermal reforming[14-15]. Alternatively, in absence of steam, chemical looping can be tailored towards partial oxidation by controlling the degree of fuel oxidation via use of an appropriate carrier material or adjustment of the carbon to oxygen ratio in the fuel reactor. In one of the first studies of such a process, Ryden et al., used a Ni-based carrier in a continuously operated fluidized bed reactor for syngas generation with and without steam co-feed. They reported near complete methane conversion with H_2:CO ratio ~2, albeit at C/O ratios well above the stoichiometric ratio for partial oxidation and hence resulting in significant carbon formation[16]. Alleviating carbon formation by co-feeding steam in the fuel reactor resulted in higher H_2:CO ratio, indicating the onset of steam reforming and/or water gas shift activity. The issue of carbon

formation is a recurring theme with use of Ni-based carriers for chemical looping syngas generation (which is not surprising, given the substantial literature on coking of Ni-based catalysts for CPOM). Although preventive measures like steam co-feeding can abate carbon deposition[17-18], the required large amounts of steam[19] (H_2O:CH_4 = 1, stoichiometrically sufficient to perform steam reforming) carries a strong energy penalty for the process and thus counters the key objective of partial oxidation. Pröll et al., investigated the effect of air to methane ratio on thermal balancing in the system to achieve autothermal operation (i.e. a balance between the exothermic and endothermic reactions occurring in the two couple reactors)[20]. They found that combustion dominates at near stoichiometric conditions, not only strongly reducing syngas yields but also requiring a large amount of cooling. While the high reactivity of nickel as oxygen carrier, combined with its reactivity as a partial oxidation catalysts, has motivated its use as carrier material for partial oxidation, Ni suffers from coke formation, is rather expensive (albeit much cheaper than the noble metal catalysts used in CPOM), and is coming under increasing pressure due to its significant toxicity. Among the very limited number of investigations into alternative, cheaper, and non-toxic carriers, a few studies on Fe-Ce mixed oxide carriers and $LaFeO_3$ and $La_xSr_{1-x}FeO_3$ perovskites have reported promising results, albeit all of these carriers suffer from low reactivity[19, 21-24,25-26].

Building on this previous work, in the present contribution, we aim to demonstrate a viable process for syngas generation via chemical looping by systematically optimizing both the oxygen carrier and the operation of the periodic redox process to tune the C/O ratio in the fuel reactor. Towards this goal, we synthesize mixed oxides of iron and nickel with the aim of combining the high reactivity of nickel with the selective oxidation properties of iron. These Fe-Ni mixed metal oxides are supported on ceria, which is well-known for its oxygen storage capacity and, more

importantly, has in previous studies from our laboratory shown a strong enhancing effect on oxygen transport and oxygen carrying capacity of supported metals, a reduction in the sensitivity to coking, and a stabilization of both mono- and bimetallic carrier materials[27-28]. These mixed oxygen carriers are screened in the fixed-bed reactor as a function of Fe:Ni ratio to determine the optimal composition for syngas generation, and the down-selected carriers are then subjected to deep reduction and oxidation in order to identify the optimal time window for oxidation and reduction in order to optimize the syngas yield and minimize coke formation. Next, multi-cycle operation with the selected carrier at the identified conditions is used to demonstrate the feasibility of this periodic redox CLPOM process. Finally, a brief reactor modeling study is used to evaluate the feasibility of conducting CLPOM in a periodically operated fixed-bed reactor.

2. Experimental:

2.1 Oxygen Carrier Synthesis:

We have previously shown that the use of reducible oxides such as CeO_2 can strongly enhance the stability of the supported metal phase and increase its reactivity in redox processes[27-28]. It should be noted that this enhancement occurred despite the fact that ceria itself does not show significant activity for methane conversion nor does it significantly contribute to the overall oxygen storage capacity of the carrier materials (with more than 95% of the oxygen storage resulting from the supported metal) [27-28]. Based on these previous observations, we again use ceria supports in the present study and deposit the metal/s of choice on these supports using incipient wetness as a simple, cheap, and scalable technique.

The ceria support was prepared via a facile hydrothermal synthesis procedure previously adapted in our research group[29]. Briefly, 0.752 g of $Ce(NO_3)_3 \cdot 6H_2O$ (99+%, Sigma-Aldrich) were

dissolved in 8 ml DI water and 30 ml of NaOH (98+%, Sigma-Aldrich) solution (7 M) were rapidly added under vigorous stirring. After 30 min of stirring, the slurry was transferred into a 50 ml autoclave, heated to 100°C under autogenous pressure for 72 h, and then allowed to cool to room temperature. The product was washed by DI water and collected via centrifugation to remove any ionic remnants until the pH of the solution was 7. After drying the powders at 100°C overnight and calcination at 450°C for 2 h, the final product was obtained.

Mixed oxides of iron and nickel (Ni_xFe_{1-x}-CeO_2) with 40 wt.% metal loading were synthesized by incipient wetness. Ni_xFe_{1-x}-CeO_2 carriers (x = 0, 0.02, 0.12, 0.33 and 1) were prepared by dissolving the appropriate amounts of $Fe(NO_3)_3.9H_2O$ and $Ni(NO_3)_2.6H_2O$ (both 99+%, Sigma-Aldrich) in 1 mL ethanol (200 proof, Decon Labs, Inc.) to obtain a clear solution. 200 mg of support were added and stirred for 2 h. The obtained slurry was dried in a vacuum oven at 80°C overnight, and calcined at 900°C for 2 h to get the final form of the oxygen carrier material.

2.2 Oxygen Carrier Characterization:

The obtained oxygen carriers were subjected to thorough characterization in order to evaluate the structural and textural properties of the carriers. The specific surface area was determined via nitrogen sorption in a Micromeritics ASAP 2020 gas adsorption analyzer using the BET method. Prior to the measurement, the samples were degassed for 2 h at 200°C under high vacuum. After calcination at 900°C for 2 h, all the carriers were found to have surface area <8 m^2/g (table 1). The relatively low surface area of the carriers after calcination at 900°C is expected due to the limited high-temperature stability of ceria[30-33]. Actual metal weight loadings of the carriers were determined via EDAX (table 1) and are in close agreement with the nominal weight loadings.

X-ray diffraction (XRD) measurements were performed with a powder X-ray diffractometer (Phillips PW1830) in line focus mode employing Cu Kα radiation (λ = 1.5418 Å) with typical 2θ scans between 15° and 90°. Crystal phases were identified based on JCPDS cards. The results are summarized in table 1. No significant interactions between the metal phase/s and the ceria support were found for any of the Ni_xFe_{1-x}-CeO_2 carriers. At low Ni content (i.e., x = 0.02, 0.12 in Ni_xFe_{1-x}-CeO_2), Fe_2O_3 was observed to be the major phase, with $NiFe_2O_4$ as a minor phase (characterized by some very weak intensity peaks in XRD). For $Ni_{0.33}Fe_{0.67}$-CeO_2, $NiFe_2O_4$ was the only mixed metal phase detected on the CeO_2 support. For the mono-metallic carriers, i.e., Fe- and Ni-CeO_2, only Fe_2O_3 and NiO phases were detected, respectively.

For the mixed metal carriers, it is important to verify the dispersion of nickel (the minor component) in the metal phase in order to assure successful formation of a mixed metal phase. Thus, JEOL JEM-2100F high-resolution transmission electron microscope (HR-TEM) was used to determine local spatial elemental composition in the sample via electron energy-loss spectroscopy (EELS) . Figure 2 shows the EELS analysis for a typical $Ni_{0.12}Fe_{0.88}$-CeO_2 sample, indicating that nickel is well dispersed in the sample and only occurs in close proximity to iron. No independent Ni islands are observed, in agreement with XRD measurements which do not show any NiO diffraction peaks (not shown here).

2.3 Fixed-bed reactor experiments:

Oxygen carriers were subjected to reduction with methane in a fixed-bed configuration to investigate their reactivity in converting methane into syngas. 100 mg of Ni_xFe_{1-x}-CeO_2 powder was placed inside the quartz-glass tubular reactor (¼" ID), which was inserted into an electric oven (Thermo Electron Corporation – Lindberg/Blue M). The carrier bed was equipped with a

coke-resistant high temperature stable thermocouple (Super OMEGACLAD® XL Thermocouple Probes) to measure the actual bed temperature. The oven was heated to 900°C, and CH_4 (1 sccm, Grade 2.0, y_{CH4} = 16.7vol% in Ar) and simulated air (20vol% O_2 in He; 20 sccm) were flown alternatingly, resulting in the periodic reduction and oxidation characteristic for CLC. In between reduction and oxidation of the carrier the reactor was purged with argon (Grade 5.0) to assure well-defined conditions at the start of each half-cycle and avoid uncontrolled formation of potentially explosive mixtures of air and CH_4 inside the reactor. After condensation of moisture, the effluent gases were recorded using a mass spectrometer (Pfeiffer Omnistar QMS 200) and molar flowrates (n_i) were determined for all species observed during the reaction. A carbon balance was performed for all data points to assure the accuracy of the analysis, and closed within 5 – 10% error for all reported experiments.

Carbon Balance:

$$n_{CH_{4,in}} = n_{CH_{4,out}} + n_{CO_{2,out}} + n_{CO_{out}} + 0.5 \times (n_{H_{2,out}} - 2n_{CO_{out}}) \quad \ldots (1)$$

On-stream methane conversion (X_{CH4}) and cumulative carrier ($X_{carrier}$) conversion were evaluated using:

$$X_{CH_4} = \frac{n_{CH_{4,in}} - n_{CH_{4,out}}}{n_{CH_{4,in}}}, \quad X_{Carrier} = \frac{4\sum n_{CO_{2,out}} + \sum n_{CO,out}}{Total\ mol\ of\ O\ in\ carrier} \quad \ldots (2, 3)$$

Selectivity towards various species (S_i) viz. CO_2, H_2, CO and carbon (C; from methane pyrolysis) was calculated via the following equations:

$$S_{CO_2} = \frac{n_{CO_{2,out}}}{\left(n_{CH_{4,in}} - n_{CH_{4,out}}\right)}, \quad S_{CO} = \frac{n_{CO_{out}}}{\left(n_{CH_{4,in}} - n_{CH_{4,out}}\right)} \quad \ldots (4, 5)$$

$$S_{H_2} = \frac{0.5 n_{H_{2,out}}}{\left(n_{CH_{4,in}} - n_{CH_{4,out}}\right)} \ , \ S_{Carbon} = \frac{0.5\left(n_{H_{2,out}} - 2n_{CO_{out}}\right)}{\left(n_{CH_{4,in}} - n_{CH_{4,out}}\right)} \quad \ldots (6, 7)$$

As expected, total oxidation, partial oxidation and catalytic pyrolysis of methane were observed to be the dominant reactions in the system. These reactions are described by following equations, illustrated here using a generic metal "Me" as oxygen carrier (with "MeO" as the generic metal oxide):

Total Oxidation: $CH_4 + 4\ MeO \Leftrightarrow 4\ Me + CO_2 + 2\ H_2O$ … (8)

Partial Oxidation: $CH_4 + MeO \Leftrightarrow Me + CO + 2\ H_2$ … (9)

Methane Pyrolysis: $CH_4\ (+\ Me) \Leftrightarrow 2\ H_2 + C\ (+\ Me)$ … (10)

3 Results

3.1 Monometallic iron and nickel carriers

Depending on the nature of the oxygen carrier and available oxygen to carbon ratio, methane conversion typically results in a sequence of total oxidation, partial oxidation, and catalytic cracking as the carrier is successively deeply reduced and conditions on the carrier surface hence become increasingly fuel rich. In order to effectively utilize the oxygen carrier for selective partial oxidation of methane, it is hence critical to understand the product spectrum obtained at various stages of the carrier reduction. This is all the more important in a fixed-bed process, where a gradient in the oxidation state of the carrier along the bed axis can result in the onset of coking on an over-reduced carrier at the bed inlet while the carrier in the later part of the bed remains only partially reduced.

Therefore, we subject the oxygen carriers to extended reduction in methane and analyze the composition of product gas stream from the fixed-bed reactor as a function of conversion (i.e. reduction) of the oxygen carrier. Figure 3 shows the selectivity traces towards various products as a function of carrier reduction for a monometallic Fe-CeO_2 carrier. Here, carrier reduction is calculated as the ratio of the amount of oxygen lost during reduction to the total amount of oxygen stoichiometrically available in the active metal (here: iron). Thus, for iron supported on ceria, 'carrier reduction' is 0% for Fe_2O_3-CeO_2 and 100% for Fe-CeO_2. The different oxidation states of iron, calculated based on the degree of carrier reduction, are indicated with dotted vertical lines in the graph. It can be seen that upon contacting methane with fully oxidized iron (Fe_2O_3), the methane oxidation reaction proceeds with high selectivity towards CO_2 formation. Thus, as expected, a large supply of oxygen, i.e. a high oxygen to carbon ratio, drives methane conversion towards total oxidation, and the first stage of the carrier reduction—the reduction of Fe_2O_3 to Fe_3O_4—is hence very selective towards methane combustion, as well-known from chemical looping combustion studies[28, 34]. Further reduction of the carrier from Fe_3O_4 to FeO appears as a step-wise transition from unselective, total oxidation to predominantly selective partial oxidation.

Continued reduction beyond FeO to metallic iron then shows a broad plateau where partial oxidation to syngas with selectivities of >70% dominates. Virtually identical selectivities towards H_2 and CO (normalized by the stoichiometric coefficient for partial oxidation) also indicate a syngas ratio (molar ratio of H_2:CO) of ~2. Again this transition is expected, as partial oxidation stoichiometrically requires only one-fourth the amount of oxygen per mol of methane compared to total oxidation, so that with greater extent of carrier reduction, i.e. progressing depletion of the oxygen reservoir or reduced oxygen to carbon ratio, methane conversion

becomes more selective towards syngas generation. Finally, as the oxygen carrier gets completely reduced, methane cracking is favored over the essentially oxygen-free metal, which is indicated by a strong increase in H_2 selectivity along with receding CO selectivity and the onset and sharp rise of carbon formation.

These results thus indicate that the various oxidation states of a metal can indeed be used quite efficiently to steer methane conversion selectively towards different oxidation products, such as total or partial oxidation. Specifically, for efficient generation of syngas using Fe-CeO_2 carriers, both the initial period of reduction (carrier reduction < 30%), which is selective for total oxidation of methane, as well as the deep reduction (carrier reduction >75-80%), which promotes methane cracking, must be avoided. This leaves a window of optimal carrier operation of ~30-75% reduction, i.e. during reactor operation, the oxygen carrier needs to be shuttled between partially reduced and partially re-oxidized states to maximize syngas selectivity in CLPOM operation.

Figure 4 shows methane conversion and CO_2 selectivity in comparison between monometallic Fe- and Ni-CeO_2 carriers. The shaded region in figure 4b shows again the range of carrier reduction where selectivity for total oxidation is low for Fe-CeO_2, and iron-based carriers seem to be an appropriate choice for partial oxidation of methane. However, the activity for methane conversion is low in this range, as seen in figure 4a, and only rises significantly for Fe-CeO_2 reduction in excess of 80%, where undesired methane cracking (and hence strong carbon formation) sets on (cp figure 3).

In contrast to Fe, Ni is known for its high C-H scission activity[10, 35], and indeed Ni-CeO_2 shows much higher methane conversion (see figure 4a). However, this carrier shows almost exclusively selective towards total oxidation of methane over almost the entire range of carrier reduction (0-

80%; see figure 4b). At even deeper reduction, the nickel-based carrier shows good activity for partial oxidation, but this range is limited to a very small fraction of usable oxygen with a narrow window of operation for syngas generation and is hence not practical for a CLPOM process. Since metallic nickel is the most studied non-noble metal catalyst in catalytic partial oxidation of methane[36], the observation that the Ni-based carrier is essentially completely unselective for partial oxidation is noteworthy and somewhat unexpected: Apparently even relatively small amounts of NiO that are present in the carrier at high reduction suffice to completely dominate the selectivity of the reaction and steer it towards total oxidation. These results hence explain also the limited success of previous studies utilizing Ni-based carriers for a CLPOM process: While Ni—or rather: NiO—is hence one of the most active and selective oxygen carrier materials for chemical looping combustion, it is clearly a poor choice as metal for a CLPOM process.

3.2 Tailoring the metal phase: Bimetallic FeNi

Based on the observation that iron is quite selective for partial oxidation but shows poor methane conversion, whereas nickel is not selective for syngas generation but has excellent methane conversion activity, we hypothesized that an appropriate combination of these two metals might allow to reconcile these two desirable features for an efficient selective oxidation process. We hence synthesized mixed Fe_xNi_{1-x} carriers at various ratios with the aim to tailor the metal phase to produce an oxygen carrier that combines good activity for methane conversion (due to the high C-H bond scission activity of nickel) with high selectivity for partial oxidation (due to the moderate oxidation strength of iron oxides).

Figure 5a summarizes the key results in terms of CO selectivity vs carrier reduction for various Ni_xFe_{1-x}-CeO_2 carriers during extended reduction in a fixed-bed reactor at 900°C. The window of selective partial oxidation over Fe-based carriers (~30-75%) is again indicated by the shaded box. It can be seen that the Fe:Ni ratio in the metal phase has indeed a significant impact on the CO selectivity. Since (monometallic) iron shows good CO selectivity starting at ~30% carrier reduction, while (monometallic) nickel only shows a brief selective phase between ~80-95% carrier reduction, the CO selectivity of the Fe-rich carriers decreases with increasing amount of nickel. Interestingly – although not entirely surprisingly – this decrease occurs from the oxygen-rich end of the operation window, where the introduction of Ni into the comparatively oxygen-rich carrier induces a rapid drop in partial oxidation selectivity.

In parallel, however, addition of Ni also results in a significant increase in activity of the carrier, as seen in figure 5b, where the rate of methane conversion is shown vs carrier conversion for the same set of mixed Fe/Ni-carrier materials. Again, as hypothesized, addition of Ni results in the expected continuous increase in conversion with increasing Ni content. Interestingly, however, this effect is not linear, i.e. even a relatively small amount of Ni addition (e.g. $Ni_{0.12}Fe0_{.88}$-CeO_2) results already in a significant increase in activity. At the same time, this composition still maintains good CO selectivity with a higher peak CO selectivity compared to that of iron (fig. 5a), and thus seems to constitute the targeted compromise between the two desired targets, i.e., high reactivity and good selectivity.

Beyond activity and selectivity for partial oxidation, carbon formation and the syngas ratio (i.e. the relative selectivity towards CO and H_2) are important factors to consider in the carrier selection. Combining iron with nickel results in carriers that begin methane cracking at an earlier stage in the carrier reduction, as reflected in the CO selectivity fall-off at the oxygen-lean

end of the selectivity maximum. This is also seen in figure 5c which shows the syngas ratio vs carrier reduction for the Ni_xFe_{1-x}-CeO_2 carriers. For all carriers, the CO:H_2 ratio is greater than 0.5 at the oxygen rich end, as expected based on the oxygen excess and the higher reactivity of H_2 compared to CO. (Note, however, that the syngas ratio at these conditions is not a meaningful number, since the reaction mainly produces total oxidation products and the ratio of the minor products CO and H_2 is hence not truly significant). As the carrier reduction approaches ~30%, all the carriers show significant CO selectivity (see figure 5a) and the CO:H_2 ratio is close to the desired value of 0.5, essentially independent on the carrier composition (note that the monometallic Ni-CeO_2 carrier is omitted from figure 5c). As the carriers gets further reduced, CO selectivity peaks and carbon formation via methane cracking starts to dominate. Consequently, as carrier reduction exceeds ~75%, the CO:H_2 ratio drops rapidly due to the shutting off of the CO formation pathway while H_2 formation continues unabated based on methane pyrolysis.

Overall, one can see that the optimal operation window, which was ~30-75% for the monometallic Fe-CeO_2 carrier, is not strongly affected by the addition of Ni (albeit the actual partial oxidation selectivity can change significantly), and we hence chose this 30 – 75 % window to compare these carrier materials. Figure 6 summarizes this comparison by showing the integral average of the methane conversion and CO selectivity over this range of carrier reduction vs the amount of Ni in the carrier. One can see that Fe-CeO_2 shows ~70% CO selectivity over this window, however, at a rather low methane conversion ~60%. On the other extreme of the spectrum, Ni-CeO_2 shows a high methane conversion of ~90% but it is almost entirely unselective for CO formation with less than 5% CO selectivity in the entire operating window. The effect of Ni addition to Fe-based carriers now becomes quite apparent from this

graph: A small amount of Ni addition initially results in virtually no change in CO selectivity (which, due to the constant $CO:H_2$ ratio represents the syngas selectivity). With increasing amount of Ni above ~10%, however, a rapid drop-off in CO selectivity is observed. Interestingly, the trend in methane conversion is quite different: Here, even a "doping" of Fe with just ~1wt% Ni (i.e. $Ni_{0.02}Fe0_{.98}$) results in a very strong enhancement in methane conversion, and a further increase to ~ 5wt% (in $Ni_{0.12}Fe_{0.88}$-CeO_2) raises the conversion essentially all the way to the values for monometallic Ni-CeO_2 carriers.

We propose that this behavior reflects the dispersion of Ni at these low concentrations in Fe and can be explained based on the microscopic reaction mechanism: For low Ni contents, Ni is essentially atomically dispersed in the iron oxide particle (see also the EELS analysis in figure 2). These dispersed Ni atoms act as active centers for methane activation, i.e. the well documented high activity of Ni for C-H bond scission[35-36] results in high conversion of methane. Oxidation of the methane fragments formed in this step then proceeds in contact with the surrounding iron oxide and hence via "soft" oxidation towards syngas. Once a critical concentration of Ni is exceeded, however, small local Ni cluster would begin to form, which offer a sufficient number of adjacent NiO sites to catalyze the total oxidation of methane typical for Ni-based carriers, and hence rapidly reduce the overall reaction selectivity. While we lack direct evidence for this mechanism (as this Ni cluster formation is likely occurring below the resolution limit of our EELS measurements of ~10 nm), the observed behavior is fully consistent with this hypothesis and thus offers a promising guideline for similar rational tailoring of bimetallic oxygen carriers, which combine active centers for methane activation based on one metal surrounded by a "sea" of a second metal with soft oxidation capability.

The increased activity of the oxygen carriers upon nickel doping is also reflected in figure 6b which shows the on-stream time required to reduce each of these carriers from 30 – 75%. It is again evident that nickel is far superior in reactivity compared to pure iron, but doping small amounts of Ni into iron already dramatically reduces the reduction time. For example, reducing $Ni_{0.12}Fe_{0.88}$-CeO_2 in this windows at identical reactor condition occurs almost twice as fast as for monometallic Fe-CeO_2 (~6 min vs ~ 11 min.). Thus, nickel doping not only augments the methane conversion while limiting the use of toxic and expensive nickel, but it also increases the rate of the reduction reaction – a factor that can strongly influence the solid inventory and/or circulation rates in the looping process if used in a transport reactor configuration.

4 Multi-cycle CLPOM operation in fixed-bed reactor:

Based on the above discussed results, $Ni_{0.12}Fe_{0.88}$-CeO_2 was down-selected as the optimal candidate for partial oxidation of methane as it showed the most favorable combination of high activity, good partial oxidation selectivity, and minimal carbon formation. In the next step of the study, this carrier was hence subjected to multiple redox cycles of CLPOM in a fixed-bed reactor, in order to verify the predictions based on the extended reduction studies and evaluate the stability of the carrier in repeated high-temperature redox cycles.

In order to avoid methane cracking and subsequent carbon carryover in oxidation, the reduction half cycles in the periodic fixed-bed experiments were terminated once the CO concentration peaked through a maximum, using the cycle times estimated from the above described experiments as a starting value. During oxidation, the cycle times were then reduced (in initial cycles) to abate CO_2 formation in the succeeding reduction half process. As a result of this initial

optimization process of the reactor operation, the initial cycles were transient in nature (not shown) with reduction and oxidation times dynamically adjusted to maintain CO formation and progressively minimize CO_2 formation. This process took about 8 – 10 cycles, reaching a thus optimized periodic steady state with a reduction time of 6.5 min and an oxidation duration of 2.5 min.

Figure 7a shows twelve representative cycles at this periodic steady state for the cyclic reduction and oxidation of $Ni_{0.12}Fe_{0.88}$-CeO_2 at 900°C with methane and simulated air. One can see that the carrier shows stable operation as apparent from the absence of any changes in height or shape of the concentration traces with time, thus confirming the stability of the bimetallic oxygen carriers over the timeframe of the experiments. Figures 7b and c show concentration traces for a single reduction (figure 7b) and oxidation half cycle (figure 7c) for closer inspection. During the first half of the reduction phase, significant CO_2 formation occurs and methane conversion is incomplete. However, unlike during the above discussed extended reduction runs with a completely oxidized carrier, H_2 and CO are formed at high concentration right from the on-set of the reduction half process. During re-oxidation (figure 7c), a small amount of carbon carry-over is observed as apparent from the formation of CO and CO_2 due to carbon burn-off. The amount of carbon carry-over corresponds to ~3% of the carbon fed in the form of methane during the reduction half-cycle. Further optimization of the reactor operation is likely to allow further reduction of this carbon carry-over but was not attempted in this proof-of-concept study. The absence of any detectable gas phase oxygen break-through indicates the efficient re-oxidation of the carrier at high oxidation rates, as well as the intended incomplete re-oxidation of the oxygen carrier in order to maximize syngas selectivity in the subsequent reduction half cycle.

Figure 8a shows the overall methane conversion as the integral average over an entire reduction half cycle along with the (integral average) distribution of carbon between CO_2, CO and solid carbon. Overall, the above reactor operation resulted in ~78% methane conversion with a CO selectivity of ~75%, corresponding to a ~58% CO yield, while ~18% of the methane feed yielded CO_2. While these numbers may not be quite on the level desirable for an industrial syngas process, they nevertheless indicate the strong potential of this process configuration as a novel partial oxidation route. Figure 8b finally shows the syngas ratio ($CO:H_2$) over an entire reduction half cycle, demonstrating again the $CO:H_2$ ratio of 0.5 over the entire half cycle with only small deviations at the very start and end of the cycle.

The failure to completely suppress CO_2 formation at the start of a reduction cycle despite the controlled re-oxidation of the carrier merits a brief further discussion. As seen in the initial study of the monometallic Fe-CeO_2 carrier, a redox cycle operating between FeO ⇔ FeO_{1-x} should result in very high syngas yields (see section 3.1). However, the nature of the oxidation process for iron oxides makes this a futile target: While Fe_2O_3 undergoes sequential reduction to Fe_3O_4, FeO and, finally, Fe, the (re-)oxidation of iron does not follow this simple and distinct sequence of oxidation steps in series[37]. As a result, while elimination of carbon formation on partially reduced Fe carriers is a relatively straightforward task which can be achieved with appropriate process control, effectively limiting carrier re-oxidation to FeO is challenging. Yet, formation of Fe_2O_3 during re-oxidation is detrimental to syngas selectivities, as it results in total oxidation of methane and likely constitutes the cause for the initial CO_2 formation in our experiments[37].

Although further improvement of methane conversion and syngas selectivity is hence desirable, the present results show that chemical looping offers ample opportunities for tuning the reducer

reactor operation towards syngas production and underscore the importance of a rational design of engineered oxygen carriers to steer the reaction selectively towards the desired products.

5 Fixed-bed reactor calculations:

The above discussed study is based on the use of a periodically operated fixed-bed reactor rather than the circulating fluidized bed (CFB) configuration currently favored for chemical looping combustion. The preference for CFB reactors is based mainly on the excellent heat management that characterizes these well-mixed reactors, an aspect which is critical in handling the strongly exothermic carrier oxidation reaction in CLC. However, operation of fluidized beds poses its own challenges, mainly associated with the large amount of solids transport, such as carrier attrition, agglomeration and deactivation, dusting, and gas leakage, to name just a few. Hence, operation of CLC in a fixed-bed reactor (FBR) configuration has been proposed and studied as an attractive alternative, but heat management remains a challenging issue due to the strong exothermicity and thus formation of hot spots and related phenomena[38].

Unlike CLC, CLPOM operation is based on a controlled and limited oxidation of carriers and on an altered gas/solid ratio (due to the difference in reaction stoichiometry) both of which significantly reduce the exothermicity of the net reaction and hence result in a strong decrease of the adiabatic temperature rise. At the same time, cyclic operation of partial oxidation in a FBR provides an opportunity to effectively heat integrate the (typically exothermic) oxidizer reaction with the endothermic reducer reactions in the overall looping process. In fact, cyclic operation of fixed-bed reactors (in a reverse-flow configuration) has been shown to be highly efficient in achieving excellent heat-integration during autothermal operation of mildly exothermic oxidation reactions[39-42].

In order to evaluate the feasibility of CLPOM in a periodically operated fixed-bed process, we hence analyzed a fixed-bed reactor model with co-current feed of methane as fuel and air as an oxidizing gas. The analysis is based on a pseudo-homogeneous fixed-bed reactor model which was previously published by Kuipers and co-workers for conventional CLC[38] and later adapted by our group for chemical looping steam reforming[43] and dry reforming[44] processes. The primary aim of the model is to determine the maximum temperature excursion in the fixed-bed reactor, based on an analytical solution of the coupled mass and energy balances using a number of simplifying assumptions. It is assumed that the oxygen carrier in the fixed bed reacts instantaneously (i.e. with effectively infinite reaction rate) with air from its fully reduced to the fully oxidized state, i.e. we do not consider intermediate oxidation states or possible gradients in the fixed-bed. Similarly, instantaneous and complete reaction is assumed for the reduction with methane. Although neither of these two assumptions, i.e. infinite reaction rates and complete conversion, is perfectly fulfilled in our case (as seen in section 4), the analysis based on these assumptions yields a conservative estimate for the expected maximum temperature rise in fixed-bed, i.e. the analysis will over-predict the temperature maximum.

Coupling of the gas-solid reaction and convective gas flow yields two spatially separated travelling wave fronts which move through the reactor bed with different velocities: The velocity of the heat front (v_h), where heat is transferred from the fixed bed to the gas phase, and the velocity of the reaction front (v_r), where all the oxygen fed in the form of air reacts with the oxygen carrier:

$$v_h = \frac{\rho_g v_g C_{P,g}}{\varepsilon_s \rho_s C_{P,s}} \qquad \ldots (11)$$

and

$$v_r = \frac{\rho_g v_g w_{g,O_2}^{in} M_{act}}{\varepsilon_s \rho_s w_{act} M_{O_2} \xi} \quad \ldots (12)$$

(Please refer to the Nomenclature section for variable meanings). It is assumed that the heat capacities of the gas and the solid ($C_{P,g}$ and $C_{P,s}$) and the solid density (ρ_S) are constant, and that the influence of pressure drop over the fixed bed and the variation of the mass flow rate can be neglected. Since the heat of reaction (ΔH_R) and specific heat capacity of the reactants ($C_{P,g}$) are only weakly dependent on temperature over the temperature range of interest, average values for ΔH_R and $C_{P,g}$ were utilized, and the calculations are not dependent on a specific reference temperature.

Assuming furthermore that the gas phase volumetric heat capacity is negligible, the heat produced by the oxidation of the oxygen carrier is taken up entirely by the solid carrier, and the energy balance can be written as

$$\frac{\rho_g v_g w_{g,O_2}^{in}}{M_{O_2}} \left(-\Delta H_R\right) = \varepsilon_s \rho_s C_{P,s} \left(v_r - v_h\right)\left(T_{\max} - T_0\right) \quad \ldots (13)$$

Substituting equations (11) and (12) in (13) and rearranging gives the maximum temperature rise in the bed:

$$\Delta T_{\max} = \left(T_{\max} - T_0\right) = \frac{-\Delta H_R}{\dfrac{C_{P,s} M_{act}}{w_{act} \xi} - \dfrac{C_{P,g} M_{O_2}}{w_{g,O_2}^{in}}} \quad \ldots (14)$$

As already pointed out by Noorman et al., under the given assumptions, the maximum temperature rise is independent of the gas velocity, suggesting that chemical looping fixed-bed reactors should scale well and be robust against changes in production capacity[38]. The decoupling of the maximum temperature rise from the gas flow is due to the assumption that the

heat capacity of the gas phase is small in comparison to that of the solid phase, resulting in negligible convective heat transport with the gas flow. The assumption can be expected to be broadly applicable due to the large difference in the volumetric heat capacities between solids and gases. Furthermore, equation (14) is independent of the reaction rate due to the assumption of infinitely fast reactions. Noorman et al. validated the robustness of their model for CLC of methane: It was observed that as long as the rates were sufficiently fast, their analytical solution showed little sensitivity to changes in the reaction rate coefficients (even for changes by a factor of as much as 7). In our case, finite reaction rates and incomplete conversion could result in temperature increases below those predicted by this analysis, i.e., as mentioned above, the analysis yields a conservative estimate of maximum temperatures.

While previous analyses had focused on the use of different metals, here we focus on the use of different oxidation states of a single metal (Fe) for total vs partial oxidation of methane as our experimental investigation had shown that the different oxidation states of Fe rather selectively steer the reaction in the direction of combustion or syngas formation. For pure Fe carriers, CLC can be operated utilizing the transition between various oxidation states, such as, $Fe_2O_3 \Leftrightarrow Fe_3O_4$ or $Fe_2O_3 \Leftrightarrow Fe$, etc. From section 3.1 we observed that only the $FeO \Leftrightarrow Fe$ transition is selective for partial oxidation. Thus, the aim of the present analysis is to investigate three different cases with the objective to understand how utilization of different oxidation states affects the maximum temperatures to be expected in chemical looping with Fe-based carriers not only due to changes in reaction selectivity (i.e. combustion vs partial oxidation) but also due to the different utilization of the carrier material.

The three cases investigated are i) $FeO \Leftrightarrow Fe$ for partial oxidation, ii) $Fe_2O_3 \Leftrightarrow Fe_3O_4$ for total oxidation and iii) $Fe_2O_3 \Leftrightarrow Fe$ for total oxidation. For simplicity, and in a crude simplification of

our experimental observations, we assume perfectly selective reaction towards the desired reaction products in each case (i.e. total or partial oxidation produces, respectively). We then utilize eq. (14) to compare the fixed-bed temperature rise on a per-mol-of-methane basis, i.e. supplying the amount of oxygen required for oxidation of one mole of methane based on the transition between the specified oxidation states of iron for each of these cases. The redox reactions, gas/solid ratio, and heat of reactions for the three cases considered in this analysis are summarized in table 2, and figure 9 summarizes the results of the analysis in terms of temperature rise as a function of the (active) Fe content in the carrier.

As expected, the temperature rise for partial oxidation is much lower than that of total oxidation using Fe_2O_3 ⇔ Fe (fig. 9a, black vs blue curves). This can be explained by the mild exothermicity of the partial oxidation reaction compared to that of the total oxidation reaction, along with the lower gas/solid ratio for total oxidation due to the higher utilization of the oxygen carrier (Fe_2O_3 ⇔ Fe vs FeO ⇔ Fe). Since the temperature rise in FBR is a strong function of the heat capacity of the carrier bed, the gas/solid ratio (determined by the reaction stoichiometry), and of the heat of reaction, the reduced solids inventory in the fixed bed coupled with the large heat of reaction results in extremely high bed temperatures when using Fe_2O_3 ⇔ Fe for total oxidation of methane. On the other hand, the mildly exothermic partial oxidation requires comparatively large amounts of solids in the FBR which act as a heat buffer during adiabatic operation.

Figure 9b shows the overall temperature rise in an idealized scenario with 100% heat integration between the endothermic reducer and exothermic oxidizer steps (i.e. loss-free heat integration). It can be seen that FBR operation of the mildly exothermic partial oxidation would not be able to sustain the bed temperature in autothermal operation with less than ~33 wt.% active metal (i.e.

Fe) in the oxygen carriers. Moreover, it would be necessary to limit the amount of active metal to <40 – 45% in order to avoid unacceptable hot-spots when operating CLPOM in FBR. This leaves a well-defined window of operation for this process with ~35-40 wt% Fe loading, supporting our choice of a metal loading of 40 wt.% in the present study.

Going beyond partial oxidation, it is instructive to furthermore briefly compare the two total oxidation cases: Remarkably, the two cases yield vast differences in temperature maxima (by as much as an order of magnitude) despite the fact that there is less than a 15% difference in heat of oxidation. This illustrates convincingly the dominating effect of the gas/solid ratio on the maximum temperature: The heat balance in the system is strongly determined by the heat capacity of the solid, and the difference in the oxygen carrying capacity (based on the transition between the different oxidation states) results in a strong difference in gas/solid ratio (see table 2). Thus, for $Fe_2O_3 \rightarrow Fe$, almost 10-times less oxygen carrier is required to combust one mole of methane than for the $Fe_2O_3 \rightarrow Fe_3O_4$ transition. The presence of a large amount of—effectively inert—solid in the latter case results in the retention of a large portion of this heat as sensible heat in the carrier, i.e. the solid effectively buffers against excessive temperature excursions. Hence, limiting chemical looping combustion to the transition between $Fe_2O_3 \Leftrightarrow Fe_3O_4$ is not only beneficial in order to assure maximum selectivity towards total oxidation—as reflected in our measurements, see fig. 4a, and reported in the literature before[22, 28]—but also to control maximum temperatures during fixed-bed operation (albeit at the expense of an increased solids inventory)[28, 34]. Finally, it should be noted here that the "heat buffering" observed for both partial and total oxidation cases will also be beneficial for an efficient heat integration between the two half cycles in a fixed-bed process, as it minimizes the heat lost with the convective flow of the gases and hence maximizes heat retention in the bed.

Overall, this brief thermal analysis thus demonstrates that fixed-bed operation of CLPOM with CH_4 is a viable option as hot spots in the carrier bed can be avoided by controlling the active metal content and oxygen utilization in the carriers. Given the significant advantages of fixed-bed reactors over transport reactors, including much reduced mechanical stress and hence attrition of the carrier material, facilitated scale-up of fixed-bed reactors in comparison to fluidized beds, and the much greater flexibility with regard to reactor throughput, a FBR configuration clearly is the reactor configuration of choice for a CLPOM process.

6 Summary:

The abundant supply of natural gas have renewed the interest in the conversion of methane into valuable chemicals and hence in the development of more efficient and scalable processes for synthesis gas generation. The present study evaluated the application of the "chemical looping principle", i.e. the periodic oxidation and reduction of an oxygen carrier material in contact with air and a fuel, to the direct partial oxidation of methane to syngas via "chemical looping partial oxidation of methane (CLPOM)".

The main focus of the investigation was on the synthesis and application of a *rationally designed* oxygen carrier for CLPOM: By combining the high activity of nickel for C-H bond breaking with the comparatively "soft oxidation" by iron oxides, we were able to design a carrier material that showed high reactivity with methane combined with good selectivity for syngas. Mixed Ni_xFe_{1-x} oxides were synthesized across a broad range of compositions, supported on CeO_2, and evaluated in extended reduction with methane to determine their reactivity and selectivity for partial oxidation. We found that even a minor addition of Ni to Fe-based carriers strongly enhanced the reactivity of the resulting carrier without significantly affecting the syngas selectivity. However, at higher Ni content (>12%), syngas selectivity decreased sharply. We

propose that this behavior can be rationalized by the presence of isolated Ni centers at low Ni content, which initiate rapid C-H bond scission while the surrounding iron oxide surface then catalyzes the subsequent selective partial oxidation to synthesis gas. With increasing Ni content, Ni oxide clusters are formed within the mixed metal oxide, which are large enough to not only break the C-H bond but also catalyze the subsequent (unselective) oxidation on NiO, resulting in a rapid and continuous drop in syngas selectivity.

Constraining the reactor operation to control the degree of oxidation and reduction of this carrier, we were able to further limit the formation of total oxidation and methane pyrolysis products at high and low carrier oxidation states, respectively: Incomplete reduction of the carriers avoids coke formation associated with methane cracking over oxygen depleted metals, while control of the re-oxidation allows to minimize the amount of oxygen available for deep oxidation of methane.

$Ni_{0.12}Fe_{0.88}$-CeO_2 was identified as the most effective carrier material and was subsequently tested in a periodically operated fixed-bed reactor for syngas generation. Stable operation with close to 80% methane conversion and ~75% CO selectivity was attained at an syngas ratio of ~2 and minimal coke formation (<3% of methane fed). While this syngas yield is somewhat lower than reported yields in conventional catalytic partial oxidation of methane (CPOM)[10-11], the present concept not only replaces the expensive noble metal catalysts used in CPOM with inexpensive transition metals (in fact, with 90% cheap and abundant iron), but also allows operation of CPOM with air without diluting the product gases with nitrogen nor requiring an air separation unit. To the best of our knowledge, this is the highest methane conversion rate reported for a (largely) Fe-based carrier to-date. Most importantly, however, the complete temporal separation of the methane and air flows, i.e. the absence of any mixed methane/air

feeds in the process, entirely avoids the safety issue inherent in handling high-temperature mixed hydrocarbon/air streams in partial oxidation processes. The safety concerns associated with these currently constitute one of the main hurdles for broader industrial implementation of CPOM as an efficient syngas technology, and CLPOM offers a novel, elegant approach to overcome this barrier.

Finally, analysis of a simple reactor model confirmed the feasibility of conducting CLPOM with Fe-based carriers in a fixed-bed reactor configuration: Our results confirm that control of maximum temperatures should not be a major concern as long as the loading of the carrier with active metal is appropriately adjusted (with a very reasonable weight loading of ~40wt% being in the optimal range) and the degree of oxidation of the carrier is controlled in order to avoid total oxidation. This reactor configuration thus allows to avoid some of the main issues in chemical looping transport reactors, such as carrier attrition and difficult reactor scale-up, and enables a much more scalable and simple operation of this process.

Overall, the present study demonstrates that the combination of rational carrier design and selection with careful identification of appropriate (dynamic) reactor operation procedures opens up the possibility to use “chemical looping” well beyond combustion applications. While the present study was focused on the production of synthesis gas from methane streams, we are currently investigating the application of the same design procedure to a wider range of selective oxidation reactions.

Acknowledgement: Financial support by the U.S. Department of Energy's National Energy Technology Laboratory (through RDS contract DE-FE0004000) and by the National Science Foundation (CBET #1159853) is gratefully acknowledged.

Nomenclature:

C_P	Heat capacity (J/kgK)
ΔH_R	Heat of reaction (J/mol)
M_{act}	Molecular weight of reactive component in solid carrier (kg/mol)
M_{H_2O}	Molecular weight of steam (kg/mol)
T_0	Initial temperature (K)
$T_{\max}$	Maximum temperature (K)
$\Delta T_{\max}$	Maximum temperature rise (K)
v_g	Gas velocity (m/s)
v_h	Heat front velocity (m/s)
v_r	Reaction front velocity (m/s)
w_{act}	Weight fraction of reactive component in solid carrier
w_{g,H_2O}^{in}	Weight fraction of steam in the feed
ρ	Density (kg/m^3)
ε_s	Porosity

ξ Stoichiometric factor (ratio of number of moles of gas to moles of solid in the oxidation reaction)

Tables and figures:

Table 1: Summary of characterization results for Ni_xFe_{1-x}-CeO_2 carriers after calcination at 900°C. (Phases marked with asterisk (*) are minor phases).

Oxygen Carrier	BET surface area (m^2/g)	Various phases of iron and nickel detected by XRD	Ni weight loading (wt.%)	
			Targeted	Actual (EDAX)
Fe-CeO_2	3.5	Fe_2O_3, CeO_2	0 (Fe wt% = 40%)	- (Fe wt% = 42.4)
$Ni_{0.02}Fe_{0.98}$-CeO_2	2.7	Fe_2O_3, $NiFe_2O_4^*$, CeO_2	1	3.1
$Ni_{0.12}Fe_{0.88}$-CeO_2	0.7	Fe_2O_3, $NiFe_2O_4^*$, CeO_2	5	8.6
$Ni_{0.33}Fe_{0.67}$-CeO_2	3.6	$NiFe_2O_4$, CeO_2	13.78	14.5
Ni-CeO_2	7.7	NiO, CeO_2	40	40.9

Table 2: Summary of redox reactions, stoichiometric gas/solid ratio, and heat of reaction for the three different cases considered for comparison in the pseudo-homogeneous reactor model to assess the maximum temperature excursion in fixed-bed reactor. ("P.O." = Partial oxidation of methane, "T.O." = Total oxidation of methane)

Case	Reaction	Gas/solid ratio	Heat of reaction (kJ/mol, at 900°C)
$FeO \Leftrightarrow Fe$ (P.O.)	$Fe + ½ O_2 \rightarrow FeO$	0.5	-270.5
	$FeO + CH_4 \rightarrow Fe + 2 H_2 + CO$	1	248.6
$Fe_2O_3 \Leftrightarrow Fe_3O_4$ (T.O.)	$8 Fe_3O_4 + 2 O_2 \rightarrow 12 Fe_2O_3$	0.25	-950.6
	$12 Fe_2O_3 + CH_4 \rightarrow 8 Fe_3O_4 + 2 H_2O + CO_2$	0.083	149.1
$Fe_2O_3 \Leftrightarrow Fe$ (T.O.)	$8/3 Fe + 2 O_2 \rightarrow 4/3 Fe_2O_3$	0.75	-1079.6
	$4/3 Fe_2O_3 + CH_4 \rightarrow 2 H_2O + CO_2 + 8/3 Fe$	0.75	278.1

Figures:

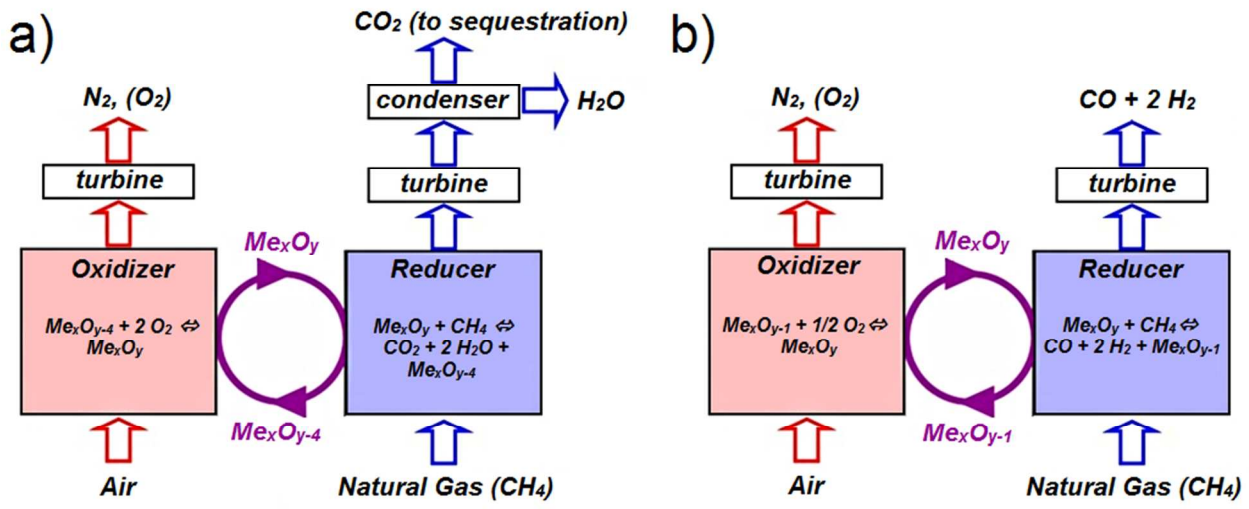

Figure 1: Simplified schematic of a) Chemical looping combustion (CLC) and b) Chemical looping partial oxidation of methane (CLPOM).

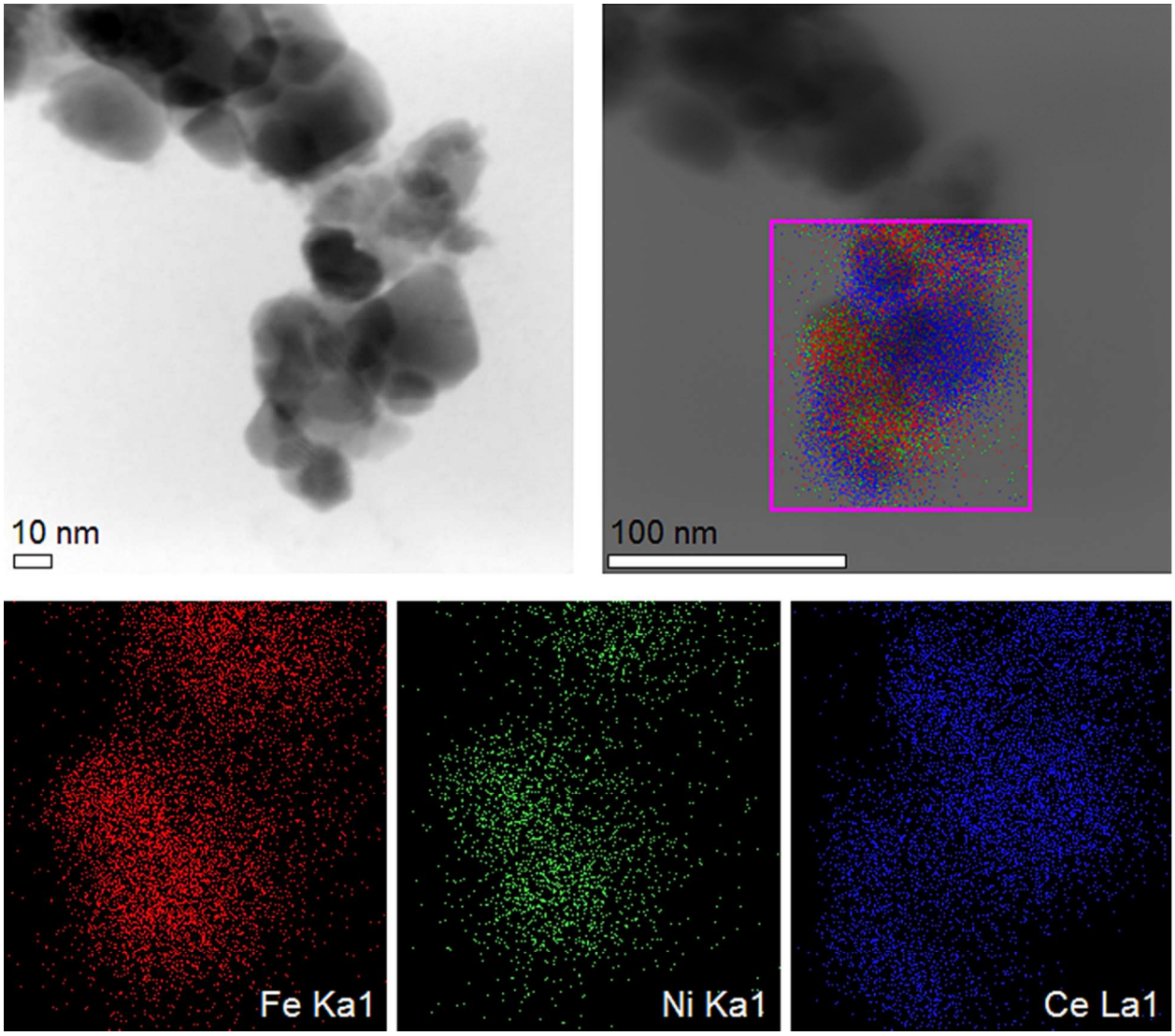

Figure 2: TEM image without (top left) and with (top right) superimposed elemental map, and elemental distribution of individual elements (bottom left: Ni, middle: Fe, right: Ce) in a $Ni_{0.12}Fe_{0.88}$-CeO_2 carrier calcined at 900°C in 0.2 SLM air for 2 h. EELS analysis confirms occurrence of iron and nickel in close vicinity at the nanometer scale.

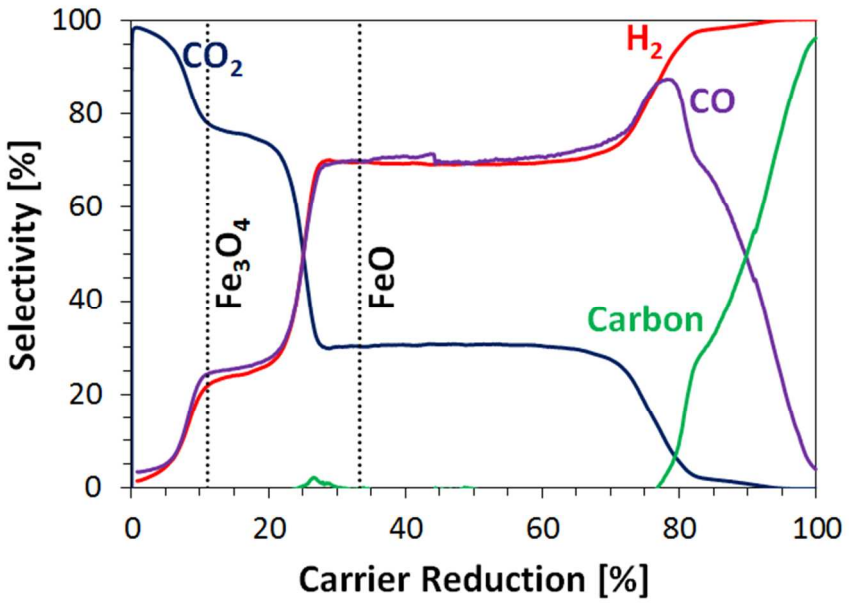

Figure 3: Selectivity towards various reaction products as a function of carrier reduction during reduction of 100 mg Fe-CeO_2 with methane (16.7 vol%, 1sccm) at 900°C.

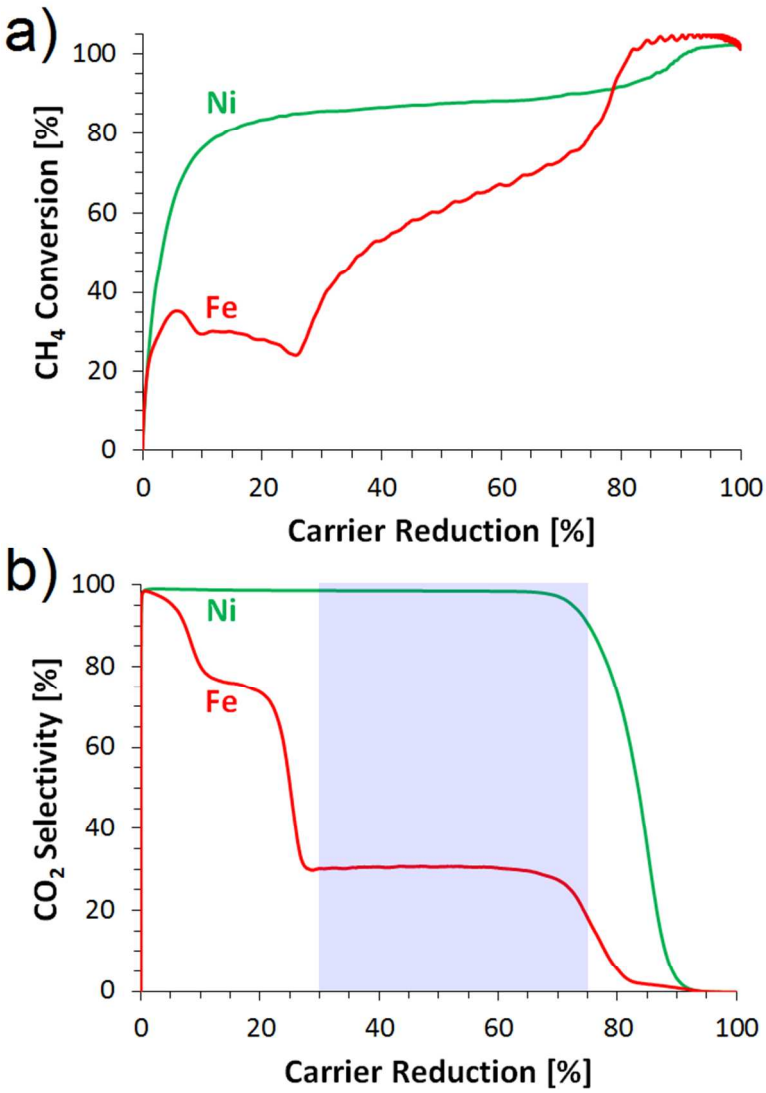

Figure 4: a) Methane conversion and b) CO_2 selectivity during reduction of Fe- and Ni-CeO_2 with methane (16.7 vol.%, 1sccm) in a fixed-bed reactor at 900°C. The shaded box in the bottom graph indicates an approximate optimal window of carrier reduction (30 – 75%) for redox cycling of Fe-CeO_2 to generate of syngas while avoiding undesired products (total oxidation and soot/coke formation).

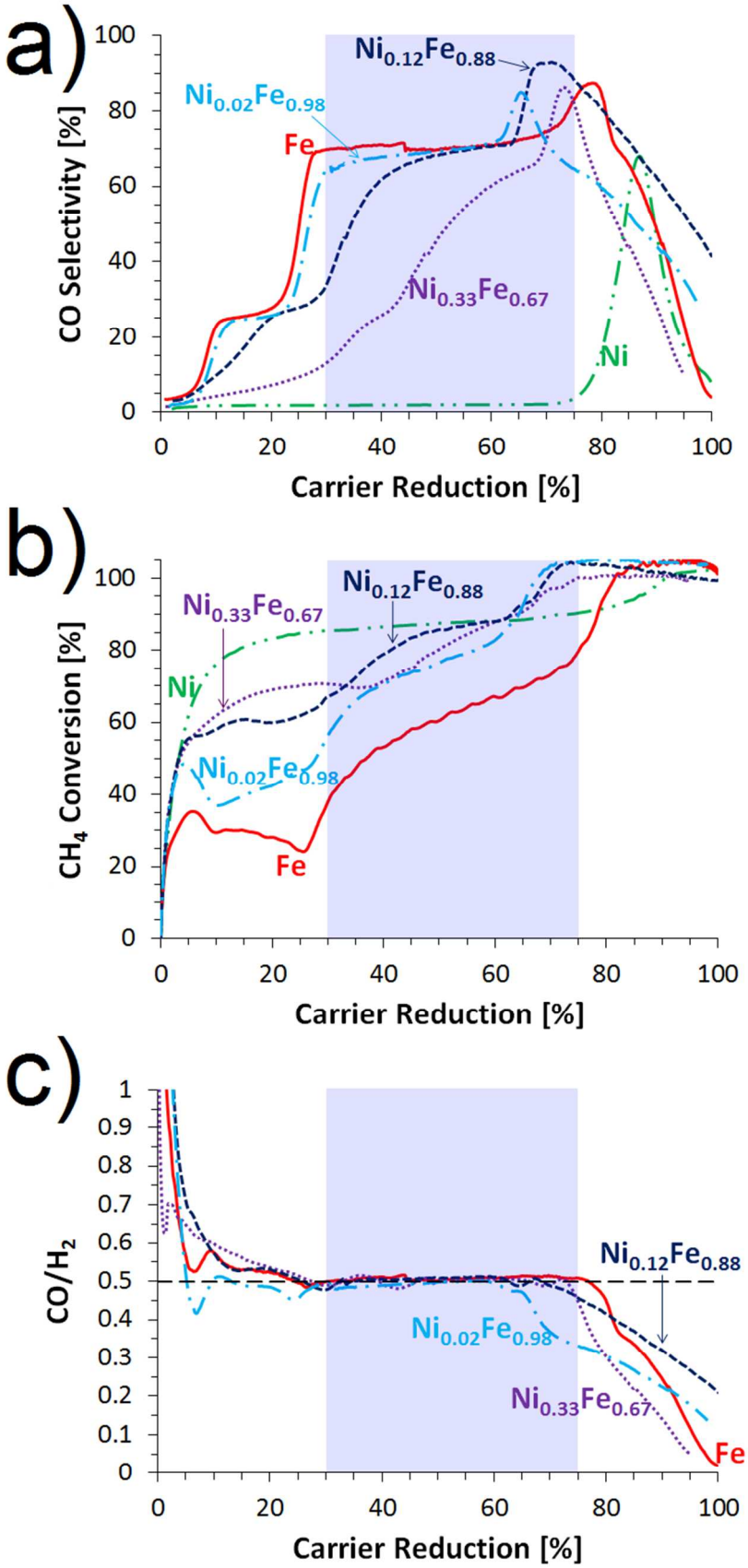
a)
CO Selectivity [%]
Carrier Reduction [%]
Ni0.12Fe0.88
Ni0.02Fe0.98
Fe
Ni0.33Fe0.67
Ni
b)
CH4 Conversion [%]
Carrier Reduction [%]
Ni0.12Fe0.88
Ni0.33Fe0.67
Ni
Ni0.02Fe0.98
Fe
c)
CO/H2
Carrier Reduction [%]
Ni0.12Fe0.88
Ni0.02Fe0.98
Ni0.33Fe0.67
Fe

685

Figure 5: a) CO selectivity, b) methane conversion and b) CO/H_2 ratio during reduction of Ni_xFe_{1-x}-CeO_2 carriers with methane (16.7 vol.%, 1sccm) in a fixed-bed reactor at 900°C. CO selectivity is a strong function of the Ni content in the mixed metal Ni_xFe_{1-x}-CeO_2 carriers. The shaded box indicates an approximate optimal window of carrier reduction (30 – 75%) in order to achieve good CO selectivity with a syngas ratio (CO/H_2) of ~0.5. (The CO/H_2 curve for Ni-CeO_2 is not shown as it does not show any significant CO selectivity in the range of carrier conversion of interest, i.e. 30 – 75% carrier reduction).

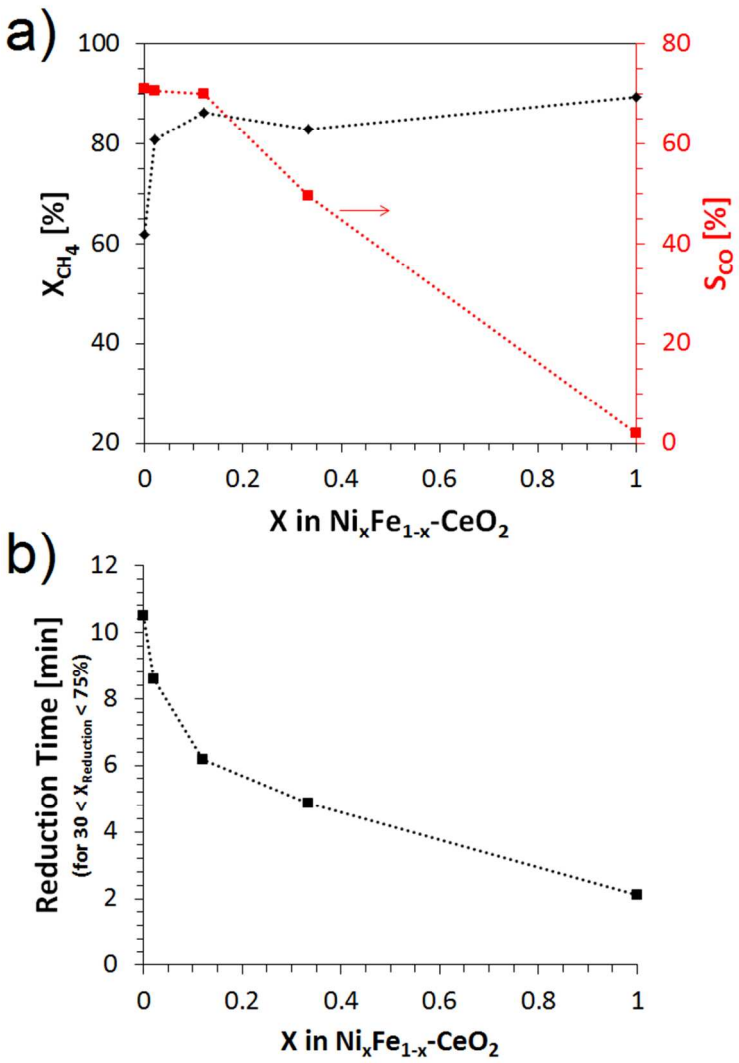

Figure 6: a) Integral methane conversion and CO selectivity, and b) time required for reduction within the optimal window for CLPOM operation (30 < carrier reduction < 75%) during reduction of Ni_xFe_{1-x}-CeO_2 carriers with methane (16.7 vol.%, 1sccm) in a fixed-bed reactor at 900°C.

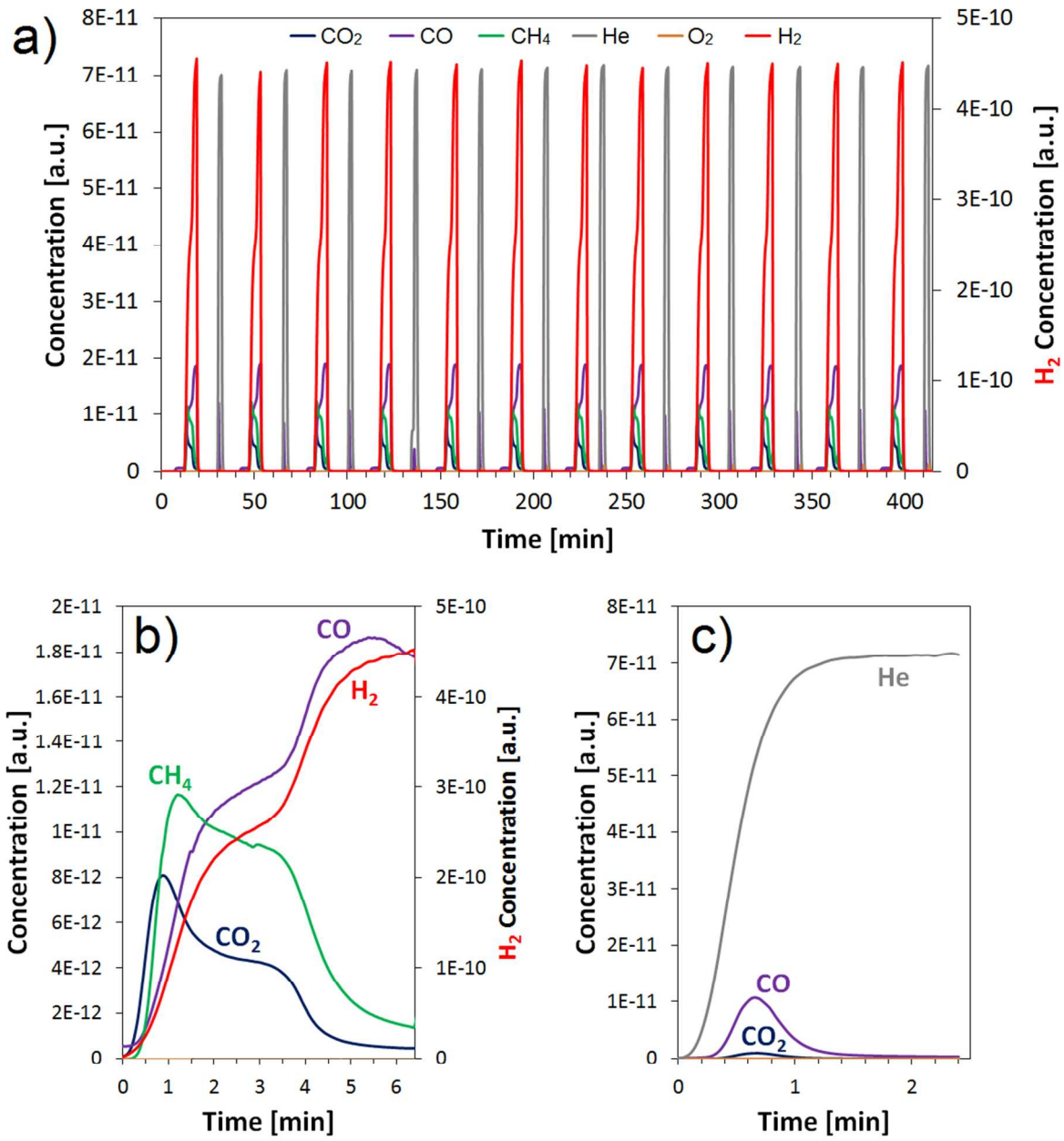

Figure 7: (a) Multi-cycle CLPOM operation with $Ni_{0.12}Fe_{0.88}$-CeO_2 at 900°C with reduction in methane (16.7 vol.%, 1sccm) and re-oxidation in 20% O_2 in He (10 sccm). Panels b and c show enlarged single reduction (b) and oxidation (c) half- cycle.

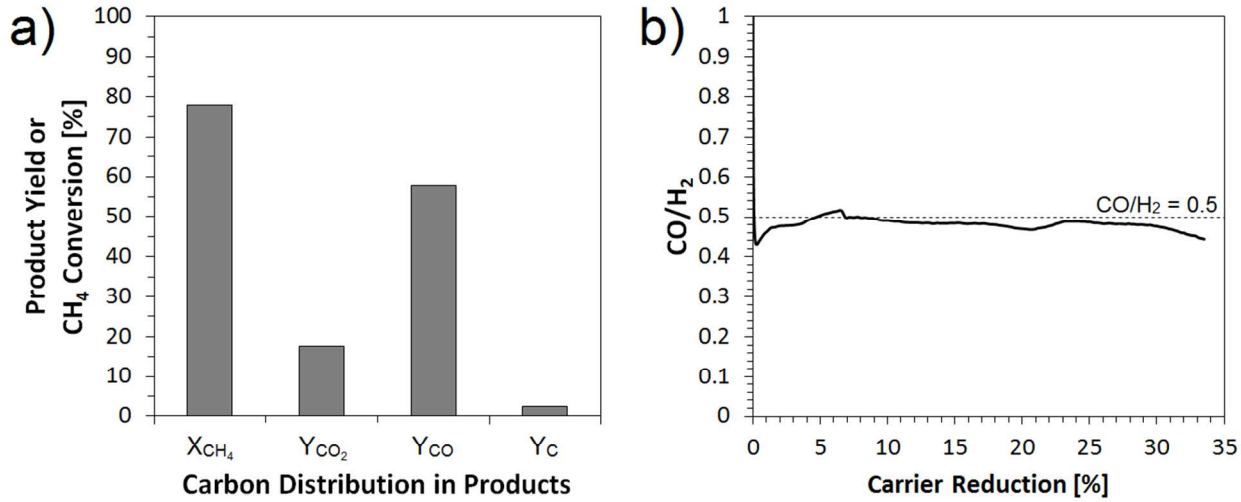

Figure 8: a) Methane conversion and product yields; b) syngas ratio (CO/H_2) during a reduction half cycle during multi-cycle CLPOM operation of $Ni_{0.12}Fe_{0.88}$-CeO_2 at 900°C.

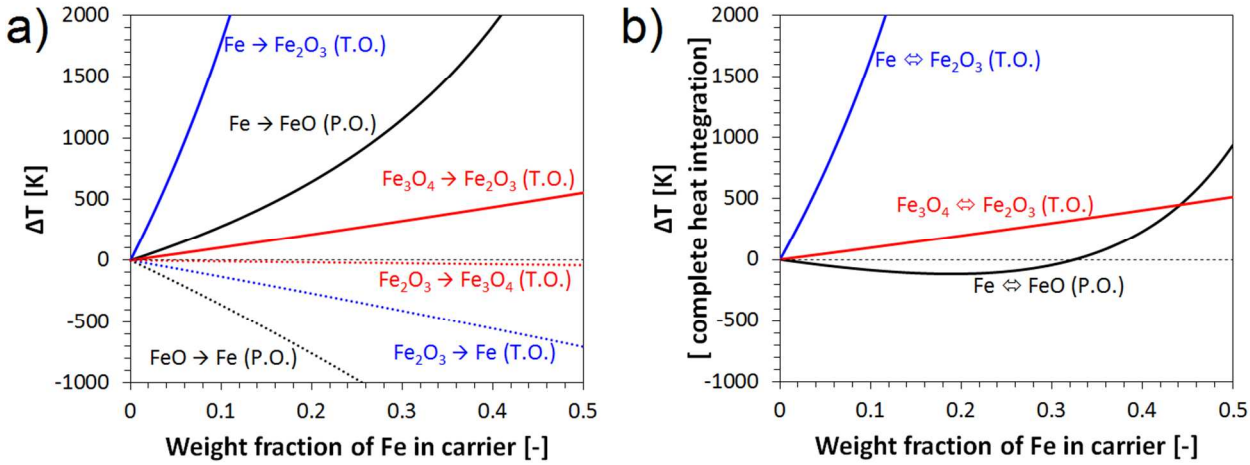

Figure 9: a) Maximum temperature rise (or drop) during reduction with methane and re-oxidation with air in a fixed-bed reactor, and b) maximum net temperature rise with idealized, loss-less heat integration between the reduction and oxidation half-cycles as a function of iron loading of the oxygen carrier ("P.O." = Partial oxidation; "T.O." = Total oxidation of methane).

References:

(1) *IEA, World Energy Outlook, 2013*; IEA: Paris, France, 2013.

(2) *US Energy Information Administration (EIA) Annual Energy Outlook*; 2012.

(3) Adanez, J.; Abad, A.; Garcia-Labiano, F.; Gayan, P.; de Diego, L. F. Progress in Chemical-Looping Combustion and Reforming technologies. *Prog. Energy Combust. Sci.* **2012,** *38*, 215-282.

(4) Hossain, M. M.; de Lasa, H. I. Chemical-looping combustion (CLC) for inherent CO2 separations-a review. *Chem. Eng. Sci.* **2008,** *63*, 4433-4451.

(5) Moghtaderi, B. Review of the Recent Chemical Looping Process Developments for Novel Energy and Fuel Applications. *Energy & Fuels* **2012,** *26*, 15-40.

(6) Anheden, M.; Svedberg, G. Exergy analysis of chemical-looping combustion systems. *Energy Conv. Manag.* **1998,** *39*, 1967-1980.

(7) Kvamsdal, H. M.; Jordal, K.; Bolland, O. A quantitative comparison of gas turbine cycles with CO(2) capture. *Energy* **2007,** *32*, 10-24.

(8) Naqvi, R.; Wolf, J.; Bolland, O. Part-load analysis of a chemical looping combustion (CLC) combined cycle with CO2 capture. *Energy* **2007,** *32*, 360-370.

(9) Wolf, J.; Anheden, M.; Yan, J. Y. Comparison of nickel- and iron-based oxygen carriers in chemical looping combustion for CO2 capture in power generation. *Fuel* **2005,** *84*, 993-1006.

(10) Hickman, D. A.; Schmidt, L. D. Production of syngas by direct catalytic oxidation of methane. *Science* **1993,** *259*, 343-346.

(11) Neumann, D.; Kirchhoff, M.; Veser, G. Towards an efficient process for small-scale, decentralized conversion of methane to synthesis gas: combined reactor engineering and catalyst synthesis. *Catal. Today* **2004,** *98*, 565-574.

(12) Ashcroft, A. T.; Cheetham, A. K.; Foord, J. S.; Green, M. L. H.; Grey, C. P.; et al. Selective Oxidation of Methane to Synthesis Gas Using Transition Metal Catalysts. *Nature* **1990,** *344*, 319.

(13) Tsang, S. C.; Claridge, J. B.; Green, M. L. H. Recent advances in the conversion of methane to synthesis gas. *Catal. Today* **1995,** *23*, 3-15.

(14) Aasberg-Petersen, K.; Bak Hansen, J. H.; Christensen, T. S.; Dybkjaer, I.; Christensen, P. S.; Stub Nielsen, C.; Winter Madsen, S. E. L.; Rostrup-Nielsen, J. R. Technologies for large-scale gas conversion. *Applied Catalysis A: General* **2001,** *221*, 379-387.

(15) Rostrup-Nielsen, J. R. Syngas in perspective. *Catal. Today* **2002,** *71*, 243-247.

(16) Ryden, M.; Lyngfelt, A.; Mattisson, T. Synthesis gas generation by chemical-looping reforming in a continuously operating laboratory reactor. *Fuel* **2006,** *85*, 1631-1641.

(17) de Diego, L. F.; Ortiz, M.; Adanez, J.; Garcia-Labiano, F.; Abad, A.; Gayan, P. Synthesis gas generation by chemical-looping reforming in a batch fluidized bed reactor using Ni-based oxygen carriers. *Chemical Engineering Journal* **2008,** *144*, 289-298.

(18) de Diego, L. F.; Ortiz, M.; Garcia-Labiano, F.; Adanez, J.; Abad, A.; Gayan, P. Hydrogen production by chemical-looping reforming in a circulating fluidized bed reactor using Ni-based oxygen carriers. *J. Power Sources* **2009,** *192*, 27-34.

(19) Zafar, Q.; Mattisson, T.; Gevert, B. Integrated hydrogen and power production with CO2 capture using chemical-looping reforming-redox reactivity of particles of CuO, Mn2O3, NiO, and Fe2O3 using SiO2 as a support. *Ind. Eng. Chem. Res.* **2005,** *44*, 3485-3496.

(20) Proll, T.; Bolhar-Nordenkampf, J.; Kolbitsch, P.; Hofbauer, H. Syngas and a separate nitrogen/argon stream via chemical looping reforming - A 140 kW pilot plant study. *Fuel* **2010,** *89*, 1249-1256.

(21) Li, K.; Wang, H.; Wei, Y.; Yan, D. Syngas production from methane and air via a redox process using Ce–Fe mixed oxides as oxygen carriers. *Applied Catalysis B: Environmental* **2010,** *97*, 361-372.

(22) Li, K.; Wang, H.; Wei, Y.; Yan, D. Transformation of methane into synthesis gas using the redox property of Ce–Fe mixed oxides: Effect of calcination temperature. *International Journal of Hydrogen Energy* **2011,** *36*, 3471-3482.
(23) Li, K. Z.; Wang, H.; Wei, Y. G. Syngas Generation from Methane Using a Chemical-Looping Concept: A Review of Oxygen Carriers. *Journal of Chemistry* **2013**.
(24) Zhu, X.; Wang, H.; Wei, Y. G.; Li, K. Z.; Cheng, X. M. Hydrogen and syngas production from two-step steam reforming of methane over CeO2-Fe2O3 oxygen carrier. *Journal of Rare Earths* **2010,** *28*, 907-913.
(25) He, F.; Trainham, J.; Parsons, G.; Newman, J. S.; Li, F. A hybrid solar-redox scheme for liquid fuel and hydrogen coproduction. *Energy Environ. Sci.* **2014,** *7*, 2033-2042.
(26) Shafiefarhood, A.; Galinsky, N.; Huang, Y.; Chen, Y.; Li, F. Fe2O3@LaxSr1−xFeO3 Core–Shell Redox Catalyst for Methane Partial Oxidation. *ChemCatChem* **2014,** *6*, 790-799.
(27) Bhavsar, S.; Veser, G. Reducible Supports for Ni-based Oxygen Carriers in Chemical Looping Combustion. *Energy & Fuels* **2013,** *27*, 2073-2084.
(28) Bhavsar, S.; Veser, G. Bimetallic Fe–Ni Oxygen Carriers for Chemical Looping Combustion. *Industrial & Engineering Chemistry Research* **2013,** *52*, 15342 - 15352.
(29) Liang, S.; Veser, G. Mixed Lanthana/Ceria Nanorod-Supported Gold Catalysts for Water–Gas-Shift. *Catal. Lett.* **2012,** *142*, 936-945.
(30) Fornasiero, P.; Balducci, G.; Di Monte, R.; Kaspar, J.; Sergo, V.; Gubitosa, G.; Ferrero, A.; Graziani, M. Modification of the Redox Behaviour of CeO2 Induced by Structural Doping with ZrO2. *Journal of Catalysis* **1996,** *164*, 173-183.
(31) Mamontov, E.; Egami, T.; Brezny, R.; Koranne, M.; Tyagi, S. Lattice defects and oxygen storage capacity of nanocrystalline ceria and ceria-zirconia. *J. Phys. Chem. B* **2000,** *104*, 11110-11116.
(32) Pengpanich, S.; Meeyoo, V.; Rirksomboon, T.; Bunyakiat, K. Catalytic oxidation of methane over CeO2-ZrO2 mixed oxide solid solution catalysts prepared via urea hydrolysis. *Appl. Catal. A-Gen.* **2002,** *234*, 221-233.
(33) Zhu, T. L.; Flytzani-Stephanopoulos, M. Catalytic partial oxidation of methane to synthesis gas over Ni-CeO2. *Appl. Catal. A-Gen.* **2001,** *208*, 403-417.
(34) Cho, P.; Mattisson, T.; Lyngfelt, A. Comparison of iron-, nickel-, copper- and manganese-based oxygen carriers for chemical-looping combustion. *Fuel* **2004,** *83*, 1215-1225.
(35) Dewaele, O.; Froment, G. F. TAP study of the mechanism and kinetics of the adsorption and combustion of methane on Ni/Al2O3 and NiO/Al2O3. *Journal of Catalysis* **1999,** *184*, 499-513.
(36) Christian Enger, B.; Lødeng, R.; Holmen, A. A review of catalytic partial oxidation of methane to synthesis gas with emphasis on reaction mechanisms over transition metal catalysts. *Applied Catalysis A: General* **2008,** *346*, 1-27.
(37) Gemmi, M.; Merlini, M.; Cornaro, U.; Ghisletti, D.; Artioli, G. In situ simultaneous synchrotron powder diffraction and mass spectrometry study of methane anaerobic combustion on iron-oxide-based oxygen carrier. *J. Appl. Crystallogr.* **2005,** *38*, 353-360.
(38) Noorman, S.; Annaland, M. V.; Kuipers, H. Packed bed reactor technology for chemical-looping combustion. *Industrial & Engineering Chemistry Research* **2007,** *46*, 4212-4220.
(39) Neumann, D.; Veser, G. Catalytic partial oxidation of methane in a high-temperature reverse-flow reactor. *Aiche J.* **2005,** *51*, 210-223.
(40) Veser, G. Multiscale process intensification for catalytic partial oxidation of methane From nanostructured catalysts to integrated reactor concepts. *Catal. Today* **2010,** *157*, 24-32.
(41) Eigenberger, G.; Nieken, U. Catalytic combustion with periodic flow reversal. *Chemical Engineering Science* **1988,** *43*, 2109-2115.

(42) Neumann, D.; Gepert, V.; Veser, G. Some Considerations on the Design and Operation of High-Temperature Catalytic Reverse-Flow Reactors. *Industrial & Engineering Chemistry Research* **2004,** *43*, 4657-4667.
(43) Solunke, R. D.; Veser, G. Hydrogen Production via Chemical Looping Steam Reforming in a Periodically Operated Fixed-Bed Reactor. *Ind. Eng. Chem. Res.* **2010,** *49*, 11037-11044.
(44) Najera, M.; Solunke, R.; Gardner, T.; Veser, G. Carbon capture and utilization via chemical looping dry reforming. *Chem. Eng. Res. Des.* **2011,** *89*, 1533-1543.